Electronic Supplementary Material (ESI) for Physical Chemistry Chemical Physics.

Computer study of the solubilization of polymer chains in polyelectrolyte complex cores of polymeric nanoparticles in aqueous media

ELECTRONIC SUPPLEMENTARY INFORMATION

Karel Šindelka[1], Zuzana Limpouchová[1*], and Karel Procházka[1*]

[1]*Department of Physical and Macromolecular Chemistry, Faculty of Science, Charles University in Prague, Hlavova 2030, 128 40 Prague 2, Czech Republic*

[*]to whom correspondence should be sent
E-mail: zl@natur.cuni.cz
E-mail: karel.prochazka@natur.cuni.cz

Table of contents:

1. Dissipative Particle Dynamics

In Dissipative Particle Dynamics (DPD) method[1, 2], the actual material (composed of solvent, ions, polymer chains, etc.) is modeled as a collection of coarse-grained spherical beads that represent lumps of the material. One DPD polymer bead corresponds roughly to one Kuhn's segment.[3] DPD beads are characterized by a mass m_i, position r_i, and velocity v_i, and interact with each other via a force F. The evolution of DPD particles in time t is governed by Newton's equations of motion:

$$\frac{d\boldsymbol{r}_i}{dt} = \boldsymbol{v}_i$$
$$m_i \frac{d\boldsymbol{v}_i}{dt} = \boldsymbol{F}_i = \sum_{i \neq j} \left(\boldsymbol{F}_{ij}^C + \boldsymbol{F}_{ij}^D + \boldsymbol{F}_{ij}^R \right) \quad \text{(S1)}$$

where the force F_i is expressed as the sum of a conservative force $\boldsymbol{F}_{ij}^C$, dissipative force $\boldsymbol{F}_{ij}^D$ and random force $\boldsymbol{F}_{ij}^R$:

$$\boldsymbol{F_i} = \boldsymbol{F_i}^C + \boldsymbol{F_i}^D + \boldsymbol{F_i}^R = \sum_{i \neq j} \boldsymbol{F_{ij}}^C + \sum_{i \neq j} \boldsymbol{F_{ij}}^D + \sum_{i \neq j} \boldsymbol{F_{ij}}^R \quad \text{(S2)}$$

The simulation run consists of a numerical solution of a set of equations S1 for all DPD beads in the simulation box with 3D periodic boundary conditions.

The forces, $\boldsymbol{F_{ij}}^D$ and $\boldsymbol{F_{ij}}^R$ arise from degrees of freedom neglected by coarse-graining and are given by

$$\boldsymbol{F}_{ij}^D = -\gamma_{ij} \omega^D \left(r_{ij} \right) \left(\frac{\boldsymbol{r}_{ij}}{r_{ij}} \cdot \boldsymbol{v}_{ij} \right) \frac{\boldsymbol{r}_{ij}}{r_{ij}} \quad \text{(S3)}$$

$$\boldsymbol{F}_{ij}^R = \sigma_{ij} \omega^R \left(r_{ij} \right) \frac{\zeta_{ij}}{\sqrt{\Delta t}} \frac{\boldsymbol{r}_{ij}}{r_{ij}} \quad \text{(S4)}$$

where $\boldsymbol{r}_{ij} = \boldsymbol{r}_i - \boldsymbol{r}_j$ is the separation vector between particles i and j, $r_{ij} = \left| \boldsymbol{r}_{ij} \right|$, $\omega^D(r)$ and $\omega^R(r)$ are weight functions that vanish for $r \geq r_c$, r_c is the cut-off radius, γ_{ij} is the friction coefficient, σ_{ij} is the noise amplitude, $\boldsymbol{v}_{ij} = \boldsymbol{v}_i - \boldsymbol{v}_j$ is the relative velocity, $\xi_{ij} = \xi_{ji}$ is a Gaussian random number with zero mean and unit variance that is chosen independently for each pair of interacting particles, and Δt is the time step. The pair-wise dissipative and random forces guarantee that momentum is conserved locally, which in turn ensures correct hydrodynamic behavior.

Forces $\boldsymbol{F_i}^D$ and $\boldsymbol{F_i}^R$ have to be well balanced with respect to each other to secure a constant temperature during the simulation run and a proper Maxwell-Boltzmann distribution of bead velocities. Espanol and Warren[4] showed that the system obeys the above requirement and samples the canonical ensemble if the fluctuation-dissipation theorem expressed by the following relationships holds:

$$\omega^D \left(r \right) = \left[\omega^R \left(r \right) \right]^2 \quad \text{(S5)}$$

$$\sigma_{ij}^2 = 2 \gamma_{ij} kT \quad \text{(S6)}$$

$\omega^D(r)$ and $\omega^R(r)$ are typically chosen[5] as

$$\omega^D(r) = \left[\omega^R(r)\right]^2 = \left(1 - \frac{r}{r_c}\right)^2 \qquad (r_{ij} < r_c)$$
$$= 0 \qquad (r \geq r_c) \tag{S7}$$

Generally, the conservative force, $\boldsymbol{F}_{ij}^{C}$, is sum of all conservative forces acting among interacting DPD particles including the electrostatic and bonding forces. The basic conservative force in DPD, $\boldsymbol{F}_{ij}^{C}$, is given as the negative gradient of a coarse-grained interaction potential, u^{CG}, acting between a pair of beads, i.e.,

$$\boldsymbol{F}_{ij}^{C} = -\nabla_{\boldsymbol{r}} u_{ij}^{CG} \tag{S8}$$

This force is purely repulsive and is derived from a soft repulsive interaction potential between the ij -pairs of particles

$$u_{ij}^{\mathrm{sr}} = \frac{a_{ij}}{2} r_{\mathrm{c}} \left(1 - \frac{r_{ij}}{r_{\mathrm{c}}}\right)^2 \qquad (r_{ij} < r_{\mathrm{c}})$$
$$= 0 \qquad (r_{ij} \geq r_{\mathrm{c}}) \tag{S9}$$

where a_{ij} is the maximum repulsion between particles i and j, r_{ij} is the separation distance, and r_{c} is the cut-off radius. Relative attraction is treated as a weaker repulsion in comparison with forces acting between other components, which is similar to the comparative description of interactions used, e.g., in the Flory-Huggins (FH) theory of concentrated polymer solutions.[6] Groot and Warren[5] mapped DPD results onto FH systems and established a link between the DPD parameters of soft repulsive forces a_{ij} and the FH interaction parameter χ_{ij}, which describes the interaction of FH segments.

$$\chi_{ij} = 2\alpha \rho r_c^3 (a_{ij} - a_{ii}) \frac{r_c}{kT} \tag{S10}$$

where ρ is the total particle density and α is a proportional constant dependent on ρ. Using the equation of state for the soft repulsive DPD fluid together with the value of compressibility for ambient water, and assuming $a_{ii} = a_{jj}$, Groot and Warren obtained an expression for like-repulsive parameters

$$\frac{a_{ii} r_c}{kT} \equiv \frac{a_{jj} r_c}{kT} = \frac{75}{\rho r_c^3} \tag{S11a}$$

The linear relationships between a_{ij} and χ_{ij} for polymeric systems at $\rho r_c^3 = 3$ results in

$$\frac{a_{ij} r_c}{kT} = \frac{a_{ii} r_c}{kT} + 3.27 \chi_{ij} \tag{S11b}$$

The system of repulsive DPD beads is confined in the simulation box with periodic boundary conditions by an implicit external force based on the experimental compressibility of the solvent, i.e., the dependence of the compressibility of the solvent on the density enables the appropriate setting of parameters of repulsive forces. In aqueous solutions, the value

a_{ij} = 25 describes favorable interactions between the components and corresponds to χ = 0, a_{ij} = 26.64 emulates the θ-state (χ = ½), a_{ij} = 33 corresponds to χ = 2.45, a_{ij} = 35 corresponds to χ = 3.06 and a_{ij} = 40 describes highly unfavorable interactions corresponding to χ = 4.59.

Polymer chains are modeled as a flexible string of DPD beads connected by elastic springs with a sufficiently high spring constant

$$u_{i,i+1}^{\mathrm{hs}} = \frac{K}{2}\left(r_{i,i+1} - r_0\right)^2 \tag{S12}$$

which act between adjacent particles i and $i+1$ in addition to the soft repulsive interaction. In Eq. (S12), K is the spring constant and r_0 is the equilibrium distance. A value of $K/(kT) = 4$ (k is the Boltzmann constant and T is the temperature) and $r_0 = 0$ were used in our simulations.

In DPD simulations of electrically charged particles (polyelectrolytes), the electrostatic conservative forces must be taken into account. The non-screened Coulomb potential (CP) describing the interaction between two point particles cannot be directly used because it diverges at short distances and, in systems that assume soft repulsive forces, it can cause the collapse of differently charged particles on top of one another. This diffuculty can be solved by cutting off of Coulomb potential or more often by smearing the electric charges. The use of the electrostatic potential between slightly smeared (slightly delocalized) charges leads to "soft" electrostatic force that does not diverge at short distances.

Several types of smearing, e.g., the linearly or exponentially decreasing charge density with the distance from the bead center, Gaussian density profile, etc., have been proposed and tested [7-10]. However, in most studies published so far, a Slater-type exponential distribution has been used [9]

$$f(r) = \frac{q\,e}{\pi\,\lambda^3}\exp\left(-\frac{2r}{\lambda}\right) \tag{S13}$$

In Eq. (S13), q is the relative charge, e is the elementary charge and λ is the decay length of the charge density. The electrostatic interaction between charged particles i and j is then given by

$$u_{ij}^{\mathrm{el}} = \frac{q_i q_j}{r_{ij}} \lambda_{\mathrm{B}} kT \left[1 - \left(1 + \beta r_{ij}\right) \exp\left(-2\beta r_{ij}\right)\right] \tag{S14}$$

where $\lambda_{\mathrm{B}} = e^2 / \left(4\pi\varepsilon_0 \varepsilon_{\mathrm{r}} kT\right)$ is the Bjerrum length (ε_0 is the dielectric constant of a vacuum and ε_{r} is the relative permittivity of the reference medium), q_i and q_j are their partial charges and $\beta = 5/\left(8\lambda\right)$. We used the decay length of the charge $\lambda = 0.2$ and Bjerrum length $\lambda_{\mathrm{B}} \cong 1.10$, which corresponds to the aqueous environment.[10] The long-range electrostatic interactions were treated using the Ewald sum with cut-off $r_{\mathrm{c}}^{\mathrm{el}} = 3$, real-space convergence parameter $\alpha^{\mathrm{ES}} = 0.975$ and reciprocal vector range $\boldsymbol{n}_{\max} = \left(5,5,5\right)$.[11] DPD trajectories were generated using the GNU program DL_MESO[12] with implemented explicit electrostatics. Simulations started always from a random configuration. After an equilibration period of $2 \cdot 10^6$ time steps, we typically ran $\left(20 - 50\right) \cdot 10^6$ time steps for associated systems and $5 \cdot 10^6$ time steps otherwise.

In the DPD method, the following reduced units were used: r_{c} is the unit of length, the unit of mass is the mass of a DPD particle and the unit of energy is kT; these terms are used throughout this work. All the DPD simulations were carried out at a total particle density of $\rho = 3$ in a cubic box of 30^3 with noise amplitude $\sigma_{ij} = 3$ and time step $\Delta t = 0.05$.

2. Definition and elucidation of calculated characteristics

The size of polymer coil in homogeneous solution is typically described by its gyration radius, which is defined as the average squared distance between monomers in a given conformation and the polymer center of mass[3].

$$R_g^2 = \frac{1}{N} \sum_{i=1}^{N} \left[\left(x_i - x_{cm}\right)^2 + \left(y_i - y_{cm}\right)^2 + \left(z_i - z_{cm}\right)^2\right], \tag{S15}$$

The gyration radius can be alternatively also expressed as

$$R_g^2 = \frac{1}{2N^2} \sum_{i=1}^{N} \sum_{j=1}^{N} \left[\left(x_i - x_j\right)^2 + \left(y_i - y_j\right)^2 + \left(z_i - z_j\right)^2\right], \tag{S16}$$

For polymer coils, the square gyration radius has to be averaged over the ensemble of allowed conformations, $\langle R_g^2 \rangle$, and this value is the most often used conformational characteristics, which can be compared with experimental values.

A more detailed description of polymer coil by the equivalent ellipsoid is based on the tensor of inertia, I. The tensor of inertia of a polymer coil is defined by means of all beads positions as [13]:

$$\begin{pmatrix} \sum_{i=1}^{N}\left[(y_i - y_{cm})^2 + (z_i - z_{cm})^2\right] & -\sum_{i=1}^{N}(x_i - x_{cm})(y_i - y_{cm}) & -\sum_{i=1}^{N}(x_i - x_{cm})(z_i - z_{cm}) \\ -\sum_{i=1}^{N}(y_i - y_{cm})(x_i - x_{cm}) & \sum_{i=1}^{N}\left[(x_i - x_{cm})^2 + (z_i - z_{cm})^2\right] & -\sum_{i=1}^{N}(y_i - y_{cm})(z_i - z_{cm}) \\ -\sum_{i=1}^{N}(z_i - z_{cm})(x_i - x_{cm}) & -\sum_{i=1}^{N}(z_i - z_{cm})(y_i - y_{cm}) & \sum_{i=1}^{N}\left[(x_i - x_{cm})^2 + (y_i - y_{cm})^2\right] \end{pmatrix} \quad \text{(S17)}$$

where the subscript cm denotes the center of mass. The values of principal moments of inertia $I_a > I_b > I_c$ can be obtained by the diagonalization of the tensor of inertia:

$$I = \begin{pmatrix} I_a & 0 & 0 \\ 0 & I_b & 0 \\ 0 & 0 & I_c \end{pmatrix}, \quad \text{(S18)}$$

The components of the gyration tensor g_a, g_b and g_c are defined as

$$g_a = \sqrt{\frac{I_b + I_c - I_a}{2N}}, \qquad g_b = \sqrt{\frac{I_a + I_c - I_b}{2N}}, \qquad g_c = \sqrt{\frac{I_a + I_b - I_c}{2N}}, \quad \text{(S19)}$$

and the square radius of gyration R_g^2 (defined by equation S15) can be represented as a sum of square components of the gyration tensor g_a, g_b, and g_c:

$$R_g^2 = g_a^2 + g_b^2 + g_c^2, \quad \text{(S20)}$$

The components of gyration tensor have also straightforward connection with the principal half-axes, l_a, l_b, and l_c, of equivalent ellipsoid:

$$l_a = \sqrt{5}\, g_a, \qquad l_b = \sqrt{5}\, g_b \qquad l_c = \sqrt{5}\, g_c, \quad \text{(S21)}$$

and each of them equals to the squared distance the whole mass of chain beads from the plane defined by principal rotational axes.

3. Elucidation of parameter setting

The copolymer PAMA-PGMA, the behavior of which we are emulating, contains the PE block based on a linear acrylic chain decorated by ionizable pendant groups attached to every repeating unit. The PAMA backbone itself is fairly hydrophobic, the short pendant

chains containing carbonyl, di(methylene) and di(methyl)amino groups are less hydrophobic, but PAMA dissolves in acidic aqueous media thanks to the protonization (ionization) of
$–N(CH_3)_2H^+$. In the PMA homopolymer, the backbone itself and the methyl group are hydrophobic, but the presence of pendant –COOH groups lowers the hydrophobicity of the repeating units and PMA is soluble in moderately acidic aqueous media when the degree of ionization is low. The solubility of PMA decreases with decreasing pH and PMA samples with molar masses $M_w > 10^4$ g/mol form loose associates at pH < 2 and easy adsorb at different surfaces and nanoparticles.[14] In our earlier DPD papers, we studied the behavior of different PEs with a hydrophobic backbone in aqueous media. In a study[15] devoted to the reproduction of pH-dependent micellization of poly(2-vinylpyridine)-block-poly(ethylene oxide) diblock copolymer, P2VP-PEO in aqueous solutions (studied experimentally in ref.[16]), we found that parameter $a = 40$ reasonably describes the interaction of the non-ionized strongly hydrophobic P2VP with aqueous media. The non-protonized P2VP is insoluble in aqueous buffers at pH > 5, where it lacks an electric charge.

In our model, we set a less solvophobic (hydrophobic) value $a_{SC} = 33$ for the DPD beads of the PE blocks. This value is based on comparison of the pH-dependent experimental behavior and DPD-emulated behavior of amphiphilic micelles with annealed PE shells, recalculated from the ionization degree-(α)-dependent to the pH-dependent behavior via a simple α-pH relationship (see our original paper[15]). Our earlier experimental studies indicated that micelles formed by symmetrical polystyrene-block-poly(methacrylic acid) are stable in the (pH – pK_A) range, which assures non-negligible ionization of PE shells α of at least 0.25.[17-19] In the simulation study focused at the behavior of micelles with PE shell-forming blocks differing in the hydrophobicity of the backbone, we found[20] that an ionization degree of $\alpha = 0.3$ represents the stabilization threshold for aqueous dispersions of micelles with $a = 32.5$. Therefore we assume that a_{SC} ca. 33 is a reasonable value for description of the interaction between PMA and the solvent beads. Because our goal is to reproduce the behavior reported by van der Burgh at a semi-quantitative level, for simplicity we used the same interaction parameters $a_{SA} = a_{SC} = 33$ for both types of PE blocks (cationic PAMA and anionic PMA) and the same value for the moderate incompatibility of PE blocks A with the neutral water-soluble block B, i.e. $a_{AB} = 33$.

However, the use of a_{SC} = 33 deserves one more comment. In the study aimed at the electrostatic co-assembly of double-hydrophilic copolymers with oppositely charged PE blocks[21], we observed that symmetrical amphiphilic copolymers (containing a non-dissociated moderately hydrophobic polyelectrolyte block with a = 35 and a water-soluble block of the same length) are molecularly soluble and do not form core/shell associates. Nevertheless, the ionization of their PE blocks and mixing with the oppositely charged diblocks triggered a pronounced co-assembling process – see Figure 4 in ref.[21] In the currently studied system, the hydrophobicity of the PAMA block is lower and the relative length of the neutral water-soluble block is larger compared to the symmetrical diblocks studied earlier. Hence the model copolymer A_5B_{15} with a non-ionized A_5 block is water-soluble and both pure components $A_5^+B_{15}$ and C_5^- dissolve in aqueous solutions, but the aqueous mixtures of ionized $A_5^+B_{15}$ with C_5^- co-assemble and form associates.

In our experimental studies[17, 22, 23], we found that the polyelecrolyte chains are usually fairly compatible with neutral water-soluble chains, e.g., poly(methacrylic acid) with poly(ethylene oxide) and therefore we set the parameters a_{BD} = a_{BC} = 25. Nevertheless, we performed also a series of simulations for a system with less compatible shell forming B block B with D and C blocks with, i.e., for a_{BD} = a_{BC} = 33.

In our model, we assume that the small counterions of either charge are fully compatible with the solvent and with the water-soluble block B (a_{SB} = 25). For the core-forming blocks, we assume that the dense insoluble cores with more or less compensated charges behave basically as a nonpolar hydrophobic medium and therefore we used the same interaction parameters for their interaction with counterions as that with water (a_{SA} =a_{SC} = 33). However, this relatively weakly repulsive interaction parameter does not prevent some penetration of the ions into the cores as a result of strong electrostatic attraction. In order to investigate the effect of parameter-setting in more detail, we performed also a series of simulations for slightly more solvophobic (hydrophobic) parameters a_{SA} =a_{SC} = a_{AB} = 35, which characterize the non-electrostatic interaction of PE beads of both A and C beads with solvent beads.

4. Proof of the appropriate equilibration of simulation results

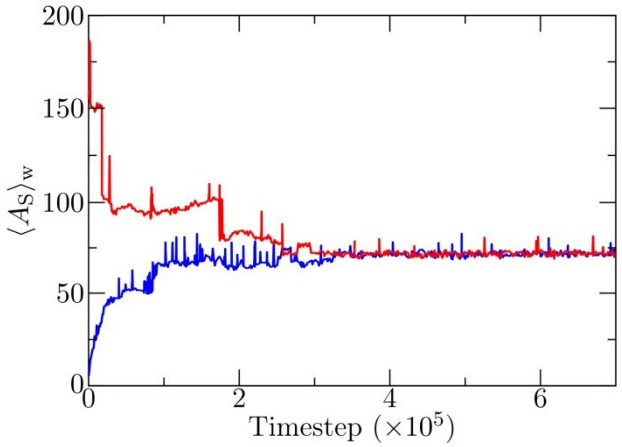

Figure S1. Simulation trajectories. Time evolution of the weight average association number, $\langle A_s \rangle_w$, formed in the system composed of 260 $A_5^+B_{15}$ and 260 C_5^- and 200 D_5 chains with interaction parameters $a_{AC} = a_{AD} = a_{BC} = a_{BD} = a_{BS} = a_{CD} = a_{BCI} = a_{SCI} = 25$; $a_{AB} = a_{AS} = a_{CS} = a_{CCI} = a_{ACI} = a_{DCI} = 33$ in two simulation runs from completely different initial conditions. Blue curve – starting from non-associated unimer chains; red curve – starting from the artificially created macroscopically precipitated system. The reasonably fast convergence of both curves to the same average value indicates a proper equilibration of the studied system.

5. Speciation diagram according van der Burgh et al.[24]

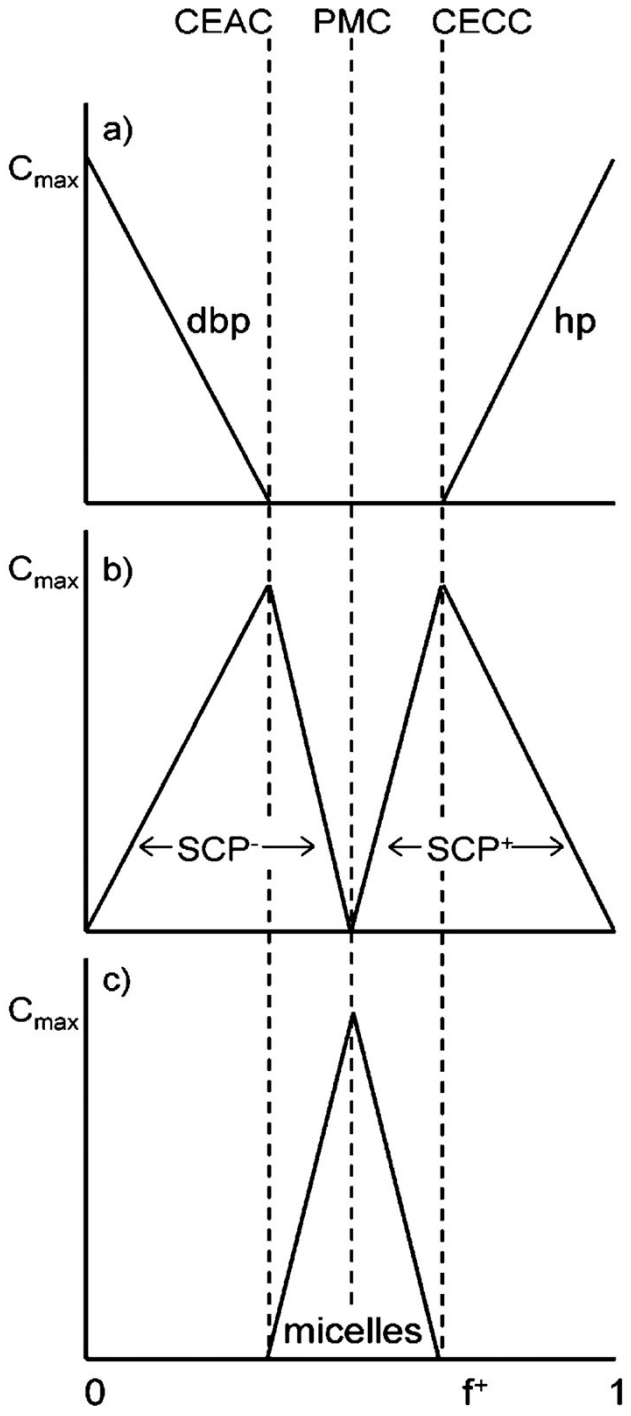

Figure S2. Speciation diagram (SD) of a mixture of homopolymer (hp) and oppositely charged diblock coppolymer (dbp). It shows the concentrations of coexisting species as a function of composition expressed as the ratio of concentrations of positively charged chains to the sum of positively and negatively charged chains in the mixture, f^+. Panel (a) shows the concentration of free polyelectrolyte molecules, panel (b) shows the concentration of relatively small and charged soluble complex particles (SCP^+, SPC^-), and panel (c) shows

the concentration of large neutral C3M micelles at constant overall concentration. The critical excess anionic charge (CEAC), critical excess cationic charge (CECC), and preferred micellar composition (PMC) are indicated by dotted vertical lines. Reproduced with the permission of the American Chemical Society (Copyright *Langmuir* **2004**, 20, 1073-1084.)

6. Supplementary data on the studied system

6.1. System without added D chains

The following part present supplementary data are for systems with interaction parameters: $a_{BC} = a_{AC} = a_{BS} = a_{SCI} = a_{BCI} = 25$; $a_{SA} = a_{SC} = a_{CCI} = a_{ACI} = a_{AB} = 33$, i.e., for systems described in the main paper.

6.1.1. Composition distributions of the highly populated associates.

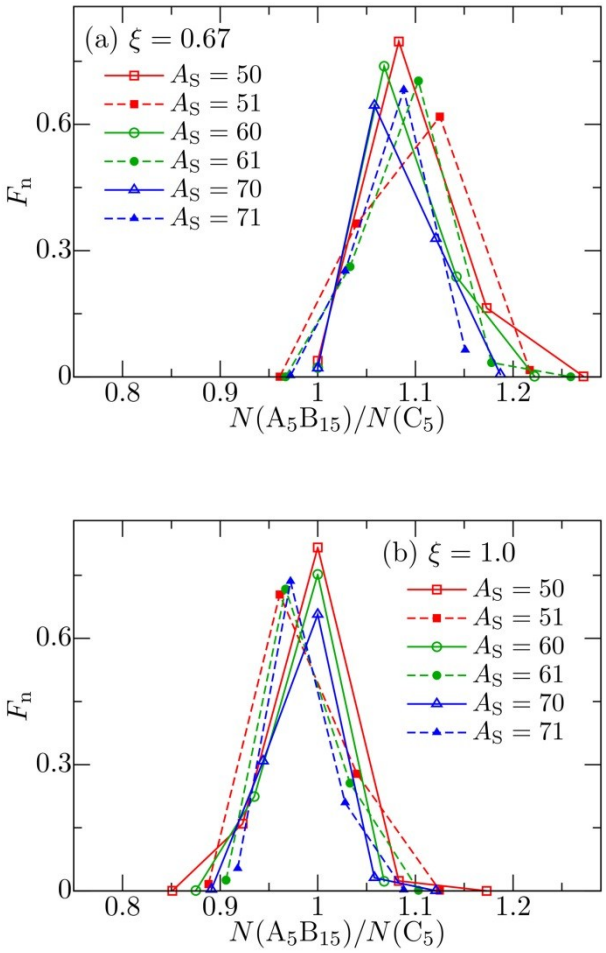

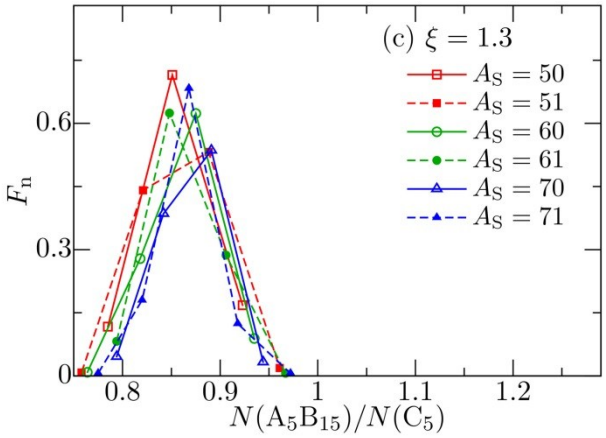

Figure S3. Distributions of number fractions, F_n, of highly populated associates with $A_S \in \langle 50, 71 \rangle$ differing in the ratio of associated chains, $\xi_{as}^{-1} = N_{A5+B15}/N_{C5-}$ in stoichiometric and non-stoichiometric systems at several ratios of negative to positive charges in the simulation box, ξ: (a) ξ=0.67, (b) ξ=1.0 and (c) ξ=1.3; A_S = 50 (solid red curve), A_S = 51 (dashed red curve), A_S = 60 (solid green curve), A_S = 61 (dashed green curve), A_S = 70 (solid blue curve) and A_S = 71 (dashed blue curve). Because the length (and therefore the weight) of N_{A5+B15} is four time larger than that of N_{C5-}, we plot the weight fractions F_n vs $N(A_5^+B_{15}^-)/N(C_5^-)$, i.e., vs ξ_{as}^{-1}.

The distributions of associates with a given association number, A_S, as functions of $N(A_5^+B_{15}^-)/N(C_5^-)$ are very narrow, i.e., the composition of highly populated associates is almost constant. Individual points in distributions differ by one added positive chain and one detracted negative chain. E.g., in the system with A_S = 60 and ξ = 1, they correspond to ratios 28/32, 29/31, 30/30, 31/29 and 32/28. This distribution (for A_S = 60 and ξ = 1) shows that that the associates with 28/32 and 32/28 are not populated at all. In systems with ξ = 1, the sets of distributions for even and odd association numbers slightly differ. The distributions for even A_S peak at ξ = 1, because neutral associates are the most favorable species from the thermodynamic point of view. The distributions for odd A_S peak at $\xi \neq 1$ simply because they cannot contain the same numbers of positively and negatively charged chains and therefore they do not contain points at ξ = 1.

In non-stoichiometric mixtures, the peak positions vary with A_S. In agreement with conclusions drawn from Fig. 2 in the main paper, the compositions of the most populated associates differ from the composition of the mixture. For ξ = 0.67, the ratio of the charged components, ξ_{as}, in highly populated associates ranges from 0.88 to 0.95 and for ξ = 1.3, it ranges from 1.1 to 1.17.

6.1.2. Radial distribution profiles

In order to illustrate the structure of pure co-assembled particles (without solubilized homopolymer chains) and of their IPC cores and the formation of charged layers at the core/shell interface in non-stoichiometric systems in more detail, below we present the radial density profiles of four systems differing in ξ. In main paper, only the results for ξ=1.81 are presented in Figure 3.

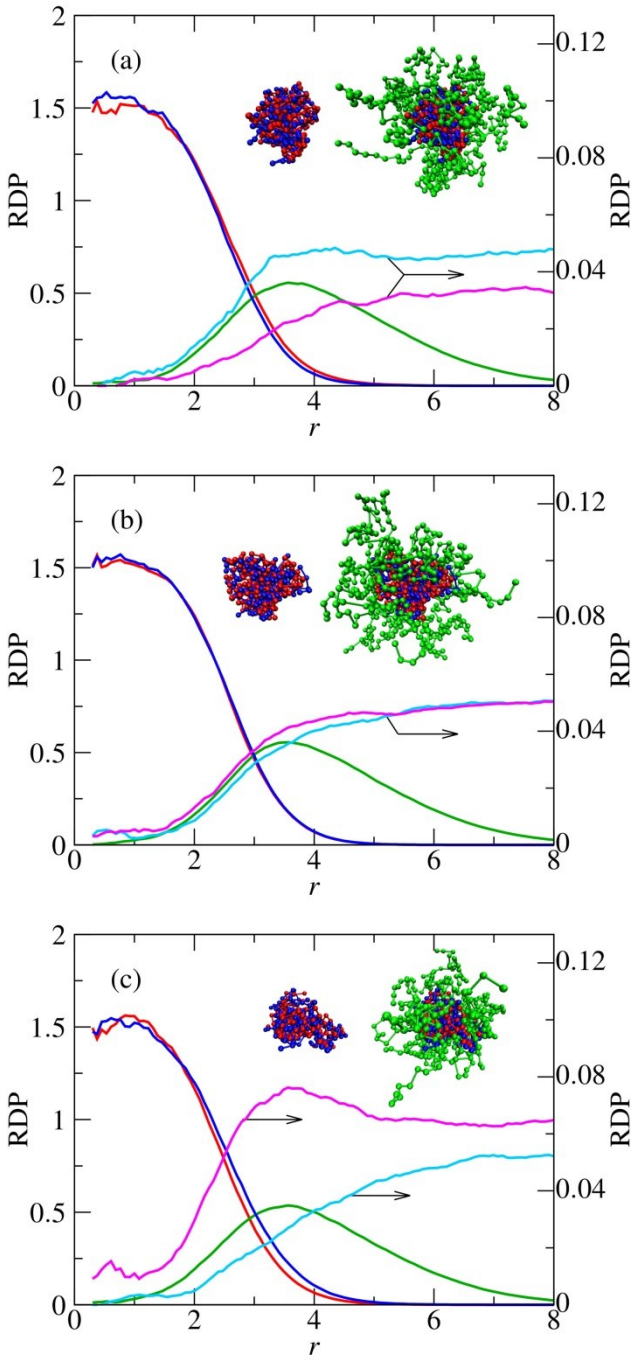

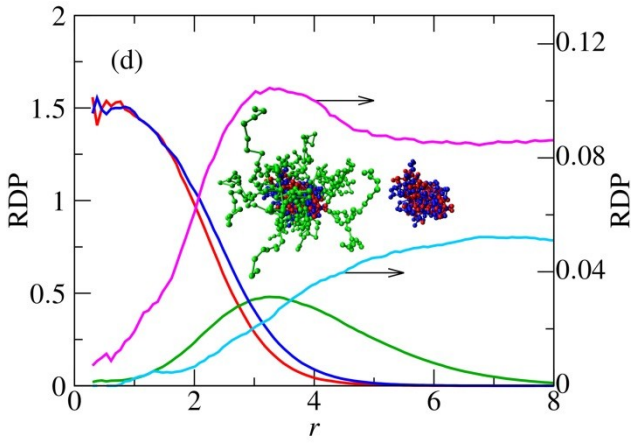

Figure S4. Radial density profiles for associates with A_s=60 for systems containing 260 $A_5^+B_{15}$ chains and with charge ratio (a) ξ=0.66, i.e. 173 C_5^- chains in simulation box, (b) ξ=1.00, 260 C_5^- chains, (c) ξ=1.33, 347 C_5^- chains and (d) ξ=1.81, 470 C_5^- chains. The left-hand vertical axis and red curves correspond to A^+ beads, green ones to B beads and the blue ones stand for C^- beads. The right-hand vertical axis corresponds to the counterion: magenta to positive ones and cyan to negative ones. The same colors are used for the typical snapshots (associates and their cores) inserted in the figures.

6.1.3. The shape of the co-assembled nanoparticles and the effect of angular averaging.

Because the instantaneous shapes of associates fluctuate and the angular averaging impoverishes information on the particle shapes, we evaluated the principal components of the gyration tensor, g_a, g_b and g_c of associates and of their insoluble cores for A_s = 50 and different ξ to see if the averaging influences significantly the simulation results.

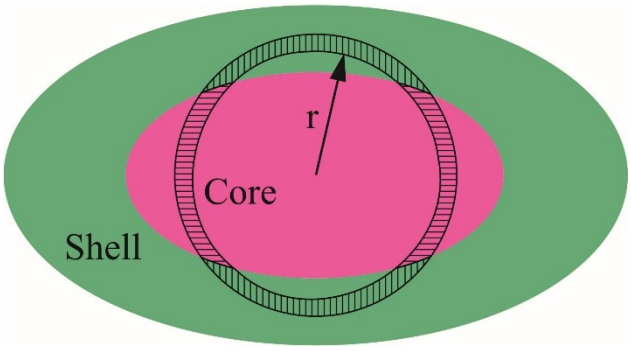

Figure S5. Scheme elucidating the problem of the evaluation of angularly averaged density profiles of core-forming and shell-forming components in a non-spherical associate with strongly segregated core (magenta color) and shell (green color). Polymer beads in the horizontally hatched magenta part of the spherical interlayer with the radius r contribute to the density profile of core-

forming component, while the beads in the vertically hatched green part contribute to the radial density profile of shell-forming component. This generates the overlap of density profiles in a certain region of r and gives false impression of the intermixing of different beads.

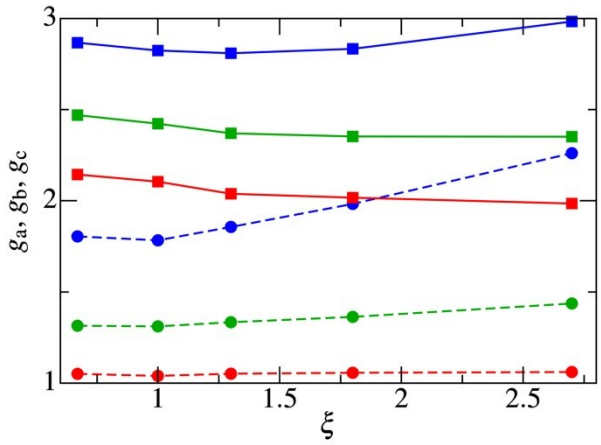

Figure S6. Principal components of the gyration tensor (g_a, g_b, g_c) for associates containing 260 $A_5^+B_{15}$ chains with A_s = 50 (solid lines) and of their insoluble cores (dashed lines) formed at different charge ratios, ξ.

The relatively close values of all three components defined by eq. S19 (ca. 1 : 1.26 : 1.72 for $\xi = 1$) in comparison with the average ensemble ratio of the axes of the ellipsoid representing the ideal chain in dilute solutions (1 : 1.6 : 3.5)[25], which almost do not change with ξ, indicate that the particles are not perfect spheres (on average they are slightly oblong ellipsoids), but the deviations from spherical symmetry are only slight. The slightly different g_a, g_b and g_c values explain the observed overlap of A and B densities in the region of distances from 1.5 to 2.5. The non-negligible overlap indicates some intermixing of A and B beads in the interfacial region, but it is augmented (see Figure S5) because the profiles become less steep as a result of the angular averaging of values for high numbers of instantaneous conformations of particles which form during the simulation run. Even though most particles can be represented by slightly prolong ellipsoids, some instantaneous shapes deviate significantly from the spherical symmetry.

6.2. Information on the solubilization of nonpolar polymer chains in IPC cores

The following part present supplementary data are for systems with interaction parameters: $a_{AC} = a_{AD} = a_{BC} = a_{BD} = a_{BS} = a_{BCI} = a_{CD} = a_{SCI} = 25$; $a_{AB} = a_{AS} = a_{CS} = a_{DS} = a_{ACI} = a_{CCI} = a_{DCI} = 33$., i.e., for systems described in the main paper.

6.2.1. Total weight fractions of solubilized chains

Weight distribution functions, $F_w(A_S)$, in mixtures containing 260 $A_5^+B_{15}$ chains and 260 C_5^- chains with D_n chains of different lengths and different fractions of D-to-(A+C) beads are shown in the main paper in Figure 5. They correspond to systems with the same number of D beads added in the form of chains with increasing length n. All the distribution curves are normalized (including the fraction of the non-associated unimer which is out of scale) and hence their visual comparison does not enable judging whether the solubilization of hydrophobic D_n chains leads to an increase in the total weight fraction of multichain associates or not. Hence, we evaluated the integrated (total) weight fractions, $\Sigma_{As} = \int_{10}^{\infty} F_w(A_S)dA_S$ of associates with $A_S > 10$ from Figure 5 in the main paper excluding the extra mass of solubilized D_n chains. The value $A_S = 10$ does not represent the absolute minimum on all the curves, but without any doubt indicates the end of the rapid initial decrease of the distribution curves in the low A_S region.

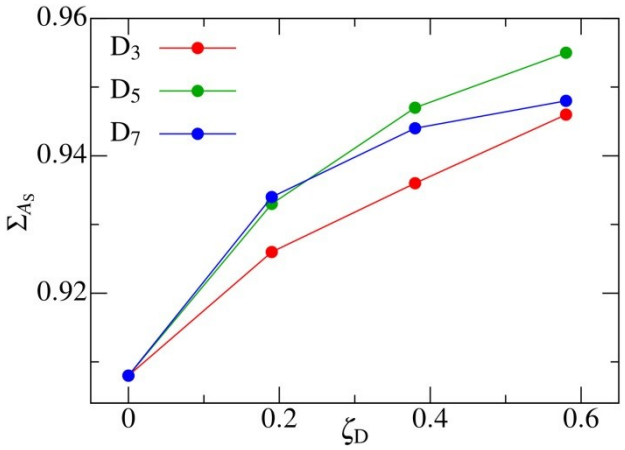

Figure S7. The integrated weight fractions of associates with $A_s > 10$, Σ_{As}, calculated from weight distribution function, $F_w(A_s)$, in mixtures containing 260 $A_5^+B_{15}$ chains and 260 C_5^- chains as function of fractions D-to-(A+C) beads, ζ_D, for different lengths n of D_n chains: D_3 red curve, D_5 green curve and D_7 blue curve. The integrated fractions do not include the solubilized chains.

The plot shows that the total (integrated) fraction of polyelectrolyte associates increases with the fraction of solubilized chains. Note that the total weight fraction does not include the weight of solubilized chains. The solubilization of longer chains (of the same length or longer than the core-forming blocks) promotes the association of $A_5^+B_{15}$ and C_5^- chains more than the solubilization of short chains. In all cases, the solubilization

effect is weak because the total fraction of large associates without the solubilized chains is fairly high (ζ_D ca. 0.9) and therefore it cannot increase appreciably. Nevertheless the increasing trend is obvious in all cases.

To summarize the effects of the length and fractions of solubilized D_n chains on the weight-average association number $\langle A_s \rangle_w$, we plotted the dependences of $\langle A_s \rangle_w$ on n and on the volume fraction of beads D in the simulation box, ν_D, in Figures S8a and S8b. Both plots clearly show that the weight-average association numbers of the associates increase with the amount and with the length of chains to be solubilized.

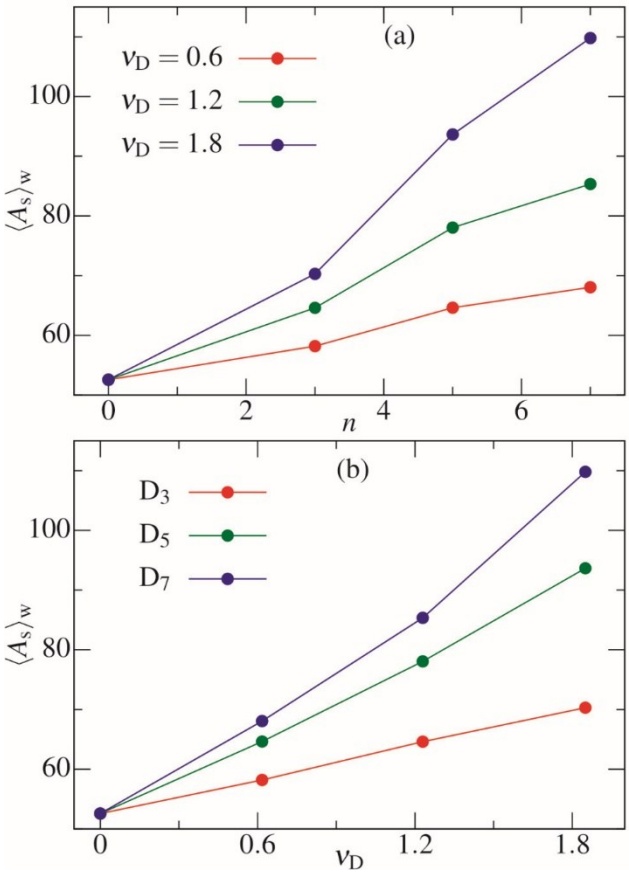

Figure S8. Weight-average association number of systems containing 260 $A_5^+B_{15}$ chains and 260 C_5^- chains (calculated only from the numbers of $A_5^+B_{15}$ and C_5^-), $\langle A_s \rangle_w$, as function of **(a)** the length n of solubilized D_n chains and **(b)** the volume fraction of beads D in the simulation box ν_D.

To finalize information on the solubilization and partitioning of chains in systems differing in total number of D beads in the simulation box and to give the reader idea on the distribution of solubilized chains of different lengths in cores of associates formed in stoichiometric mixtures, we plot in Figure S9 the ensemble-average numbers of D beads, $\langle N(D) \rangle$, solubilized in one core containing

a given number of $A_5^+B_{15}$ and C_5^- chains, $\langle N(A_5^+B_{15}) + N(C_5^-)\rangle$. As expected, the number of solubilized beads increases with the size of the core, i.e., with number of associated chains. While the increase is almost linear for the short and easily locatable D_3 chains, the plot is up-curved for long D_7 chains, which reflexes their difficult accommodation in small associates.

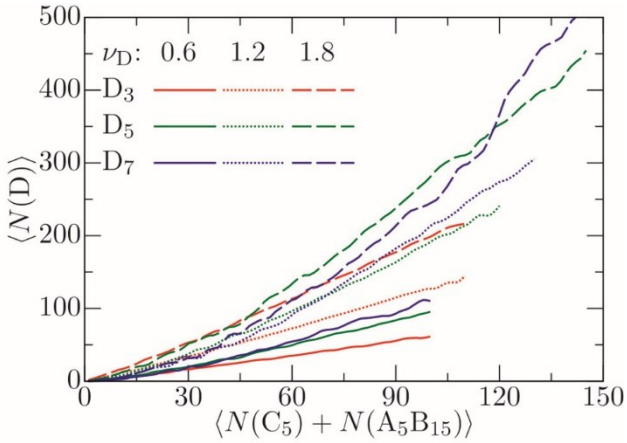

Figure S9. The average number of D beads, $\langle N(D)\rangle$, solubilized in associate with association numbers A_S (based on the numbers of assembled chains $A_5^+B_{15}$ and C_5^-, i.e., the solubilized D_n chains are not included) as a function of the average number of core forming chains $\langle N(A_5^+B_{15}) + N(C_5^-)\rangle$ in systems containing 260 $A_5^+B_{15}$ chains and 260 C_5^- chains for different length n of solubilized D_n chains and different volume fractions ν_D of added D_n chains. Volume fraction of D beads in simulation box ν_D = 0.6 Vol% corresponds to the fraction of beads D in the simulation ζ_D = 0.19 (solid lines) , ν_D = 1.2 Vol% to ζ_D = 0.38 (dotted lines) and ν_D = 1.8 Vol% to ζ_D = 0.57 (dashed lines). Red curves are for D_3 chains, green ones for D_5 and the blue ones are for D_7.

6.2.3. The effect of the length of solubilized chains on the size of cores of associates with a given association number A_S

It is interesting to investigate how the solubilization of solvophobic chains differing in length affects the size of associates with a constant A_s value and particularly the size of their cores. Figure S10 depicts a plot of the radii of the gyration of cores of associates with A_s = 60 formed in mixtures with different ξ, without and with a constant number of D beads added in the form of D_n chains with different numbers of beads n.

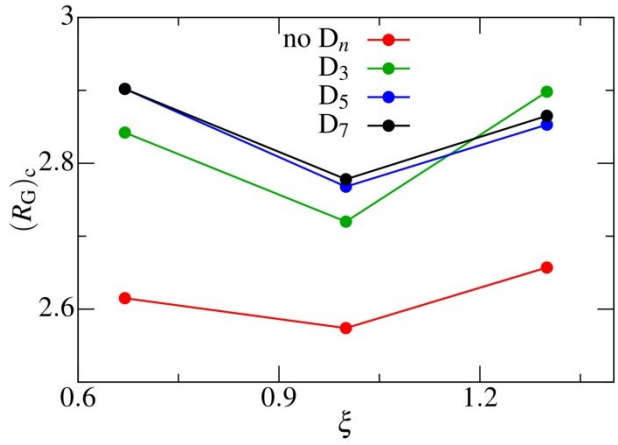

Figure S10. The radii of gyration of cores $(R_G)_c$ of associates with A_s = 60 formed in mixtures containing 260 $A_5^+B_{15}$ chains and with different ξ, without and with a constant number of D beads in the simulation box (N_D = 1000) added in form of D_n chains with different numbers of beads n.

6.2.4. The partitioning of D chains between bulk solvent and IPC cores.

In the main part of our study (for interaction parameters, see Table I in the main text), we set the interaction parameter of D_n chains with solvent the same as the moderately bad parameter describing the interaction of shell forming blocks with solvent for the following reasons: Despite the fact that we do not study the kinetics of solubilization, we wanted to address the systems which are reasonable from the experimental point of view. The electrostatically co-assembled systems currently form upon a simple mixing of solutions of oppositely charged components. It is therefore evident that a reasonably efficient solubilization of polymer chains assumes at least their marginal solubility in a given solvent. To provide information on the solution behavior of D_n chains, we evaluated the partition coefficients describing their partition between the bulk solvent and IPC cores.

Table S1. Partition coefficients $K_f = c_{D,core}/c_{D,bulk}$ as ratio of the average concentration of D beads in core, $c_{D,core}$, and in bulk, $c_{D,bulk}$ for several values of charge ratio, ξ, length n of the solubilized D_n, chains and the number of chains in simulation box, N_D . Symbol "-" denotes that the simulation data are not available.

	K_f for D_3			K_f for D_5			K for D_7		
N_D	167	333	500	100	200	300	72	143	214
ξ=0.67	-	43.3	-	-	169	-	-	666.2	-
ξ=1.00	40.2	41.2	41.9	151.9	168	185.5	501.8	616.8	739
ξ=1.33	-	31	-	-	174.4	-	-	643.4	-

The table shows that K_f increase with the increase in length of D_n chains, simply because their solubility decreases. The values are relatively low (K_f ca. 40) for short chains D_3. However, the concentration of D_3 inside the cores is still ca. 40 times higher than that in bulk solvent which indicates meaningful solubilization and accumulation of nonpolar chains in IPC cores. The partition coefficients are not constant and increase with increasing number of D_3 chains in the box. The increase in K_f is caused by the fact that A_s and the size of associates increases upon the solubilization (see Figure 5 in the main paper and S10). As it can be expected from previous parts, the values of K_f depend also on ξ. A markedly decreased K_f for D_3 and ξ = 1.33 (K_f ca. 30) is caused by the already mentioned shift of the distribution function of associates towards lower A_s upon the solubilization of short chains in non-stoichiometric co-assemblies with the excess of C_5^-. As shown in previous parts, we study non-frozen (kinetically mobile) systems and both the ratio of charged components ξ and the number of added D_n chains, N_D, and their length, n, affect appreciably the distribution of association numbers (see Figures 5 and 7 in the main paper). K_f for longer chains are higher (K_f ca. 600 for D_7) and depend also on N_D and ξ. For D_5 and D_7 they pass through shallow minima at ξ =1. Because the volume of bulk solvent is significantly larger than that of IPC cores, the ratio of chains dissolved in bulk to chains in cores, i.e., the distribution coefficient $K_{disrt} = N_{D,core}/N_{D,bulk}$ is naturally smaller than K_f, i.e., K_{disrt} for D_7 is ca. 0,03. Just to relate the amounts of D_n in cores and in bulk solvent with the amounts of hydrophobic compounds solubilized in real polymeric micelles, it is noteworthy that,

e.g., the experimental value of the partition coefficient of strongly non-polar (and almost water insoluble) pyrene between polystyrene cores of polystyrene-*block*-poly(methacrylic acid) micelles and aqueous phase[26] is K_f ca. 10^6, but because the ratio of volumes of polystyrene cores and water in a solution with concentration 1 mg/mL is ca. 10^{-6}, the same amounts of pyrene molecules are distributed in both phases, i.e., $K_{disrt} = 1$.

7. Simulations for systems with slightly changed parametes

7.1. Simulations for systems with less soluble beads A and C.

This part contains data for the system with $a_{BC} = a_{BD} = a_{AC} = a_{AD} = a_{BS} = a_{CD} = a_{BCI} = a_{SCI} = 25$; $a_{SA} = a_{SC} = a_{SD} = a_{AB} = a_{CCI} = a_{ACI} = a_{DCI} = 35$.

In order to investigate how the decreasing hydrophilicity and consequent decreasing solubility of A and C blocks affect the co-assembly, we performed a series of simulations for systems with $a_{AB} = a_{AS} = a_{CS} = 35$. As it can be expected, the tendency towards the co-assembly is more pronounced in systems with $a_{AB} = a_{AS} = a_{CS} = 35$ than in systems with $a_{AB} = a_{AS} = a_{CS} = 33$. The results of simulations for $a_{AB} = a_{AS} = a_{CS} = 35$ confirm the basic features observed for the systems with $a_{AB} = a_{AS} = a_{CS} = 33$, but we see some interesting differences. The associates with the highest A_s are formed in the system with matched ratio of negative to positive charges, $\xi = 1$. However, non-negligible fractions of multi-chain associates with fairly high A_s are formed in systems with $a_{AB} = a_{AS} = a_{CS} = 35$ for $\xi = 0.19$ and $\xi = 2.7$. Note that associates with large A_s do not exist for corresponding ξ values in the system with $a_{AB} = a_{AS} = a_{CS} = 33$. This observation demonstrates that the span of the CEAC – CECC region (critical excess anionic/cationic charge – proposed by van der Burg[24]) depends sensitively on the hydrophilicity/hydrophobicity of polyelectrolyte chains forming the inter-polyelectrolyte complex core of associates. Because the data for $a_{AB} = a_{AS} = a_{CS} = 35$ were simulated only for the sake of comparison with data for $a_{AB} = a_{AS} = a_{CS} = 33$ in ESI, the statistics is worse than that of data presented in the main paper for $a_{AB} = a_{AS} = a_{CS} = 33$.

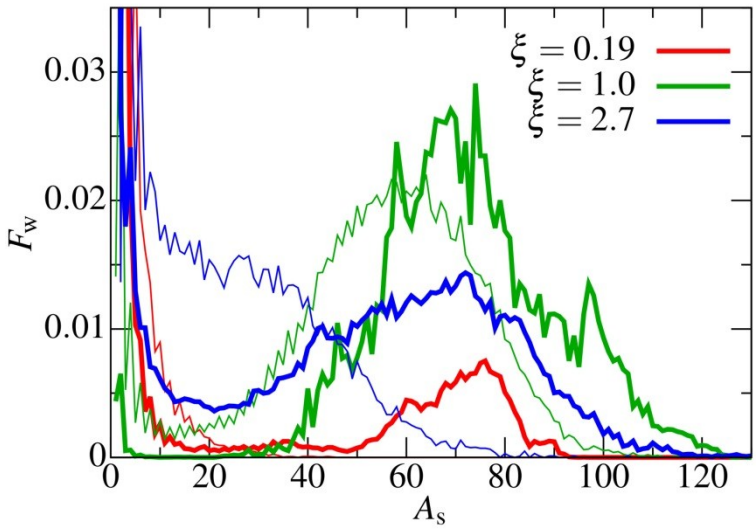

Figure S11. Weight distribution function, $F_w(A_S)$, of co-assembled particles in mixtures with several ratios of negative to positive charges, ξ, for $a_{AC} = a_{BC} = a_{BS} = 25$ and $a_{AB} = a_{AS} = a_{CS} = 35$ (thick curves) and $a_{AB} = a_{AS} = a_{CS} = 33$ (thin curves).

7.2. Simulations for systems with less compatible beads B with D and C.

The following part present supplementary data are for systems with interaction parameters: $a_{AC} = a_{AD} = a_{BS} = a_{CD} = a_{BCI} = a_{SCI} = 25$; $a_{AB} = a_{AS} = a_{BC} = a_{BD} = a_{CS} = a_{DS} = a_{CCI} = a_{ACI} = a_{DCI} = 33$.

Because polymers differing in chemical nature are generally incompatible, we investigated how a slightly worse compatibility of the shell-forming blocks with D and C chains affects the solubilization process and the structure of IPC cores with solubilized chains. Therefore we changed a_{BC} and a_{BD} parameters to $a_{BC} = a_{BD} = 33$. Selected results for non-stoichiometric mixtures with the charge ratio ξ=0.66, 1.00 and 1.33 are compared with the systems with compatible polymer species in Figures S12, S13 and S14, respectively. For more details on the lengths of chains, etc., see the Figure Caption. The comparison shows that the moderate incompatibility does not prevent the solubilization of solvophobic chains in IPC cores. In a system with less compatible blocks, the distribution functions of weight fractions slightly shift to lower A_S and the *RDPs* indicate that the homopolymer chains concentrate more in the central part of the IPC core, however they are still significantly intermixed with the core-forming chains.

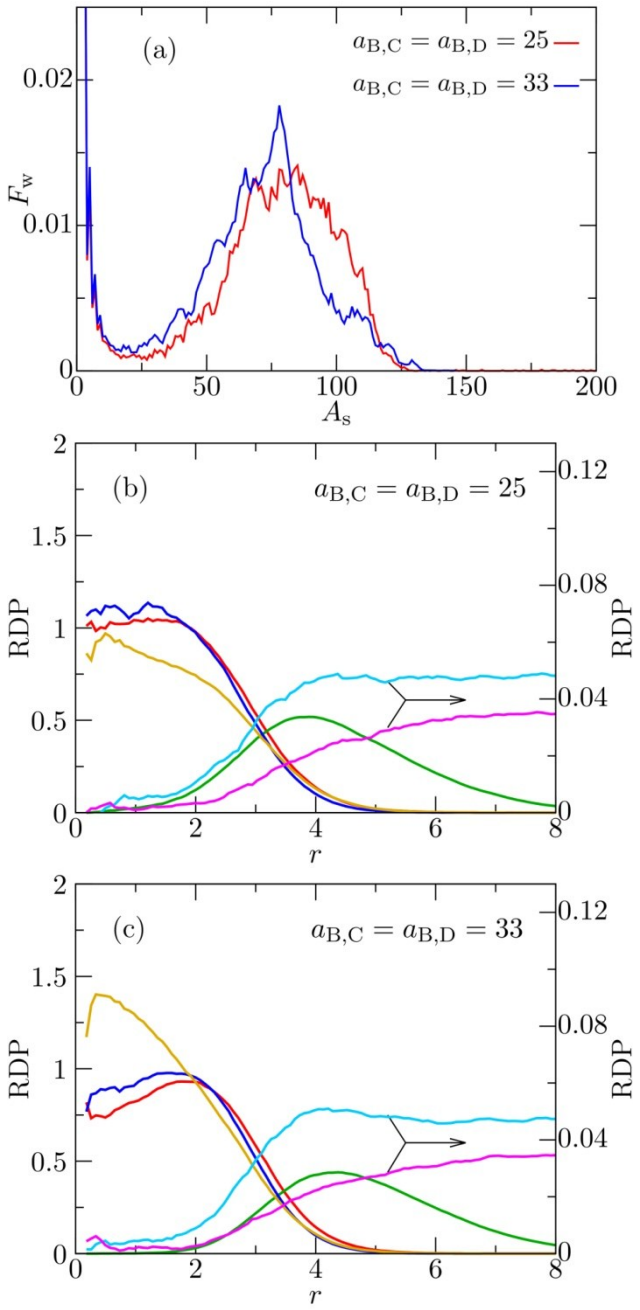

Figure S12. Systems containing 260 $A_5^+B_{15}$ chains, 173 C_5^- chains (charge ratio ξ=0.66) and 200 D_5. Part (a) Weight distribution function, $F_w(A_S)$, of co-assembled particles in mixtures with $a_{BC} = a_{BD} = 25$ (red curve) and $a_{BC} = a_{BD} = 33$ (blue curve). Parts (b) and (c) Radial density profiles for associates with A_S=60 for (b) $a_{BC} = a_{BD} = 25$ and (c) $a_{BC} = a_{BD} = 33$. The left-hand vertical axis and red curves correspond to A^+ beads, green ones to B beads, the blue ones stand for C^- beads and the ochre ones for D beads. The right-hand vertical axis corresponds to the counterion: magenta to positive ones and cyan to negative ones.

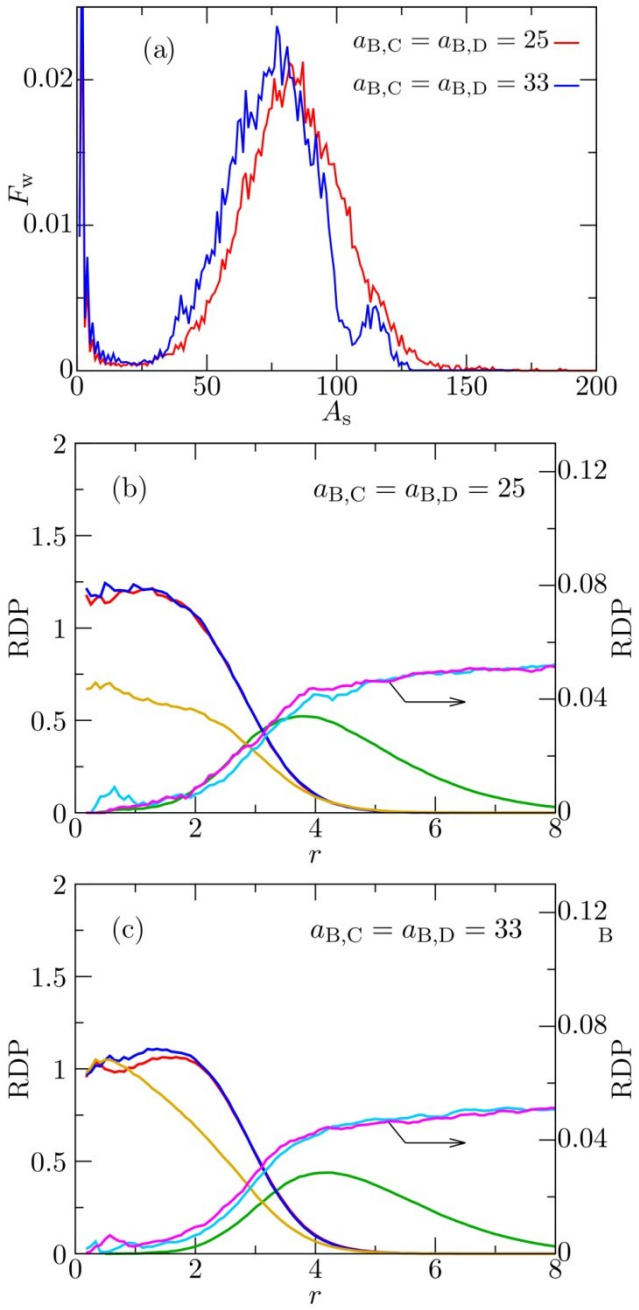

Figure S13. Systems containing 260 $A_5^+B_{15}$ chains, 260 C_5^- chains (charge ratio ξ=1.00) and 200 D_5. Part (a) Weight distribution function, $F_w(A_S)$, of co-assembled particles in mixtures with $a_{BC} = a_{BD} = 25$ (red curve) and $a_{BC} = a_{BD} = 33$ (blue curve). Parts (b) and (c) Radial density profiles for associates with A_S=60 for (b) $a_{BC} = a_{BD} = 25$ and (c) $a_{BC} = a_{BD} = 33$. The left-hand vertical axis and red curves correspond to A^+ beads, green ones to B beads, the blue ones stand for C^- beads and the ochre ones for D beads. The right-hand vertical axis corresponds to the counterion: magenta to positive ones and cyan to negative ones.

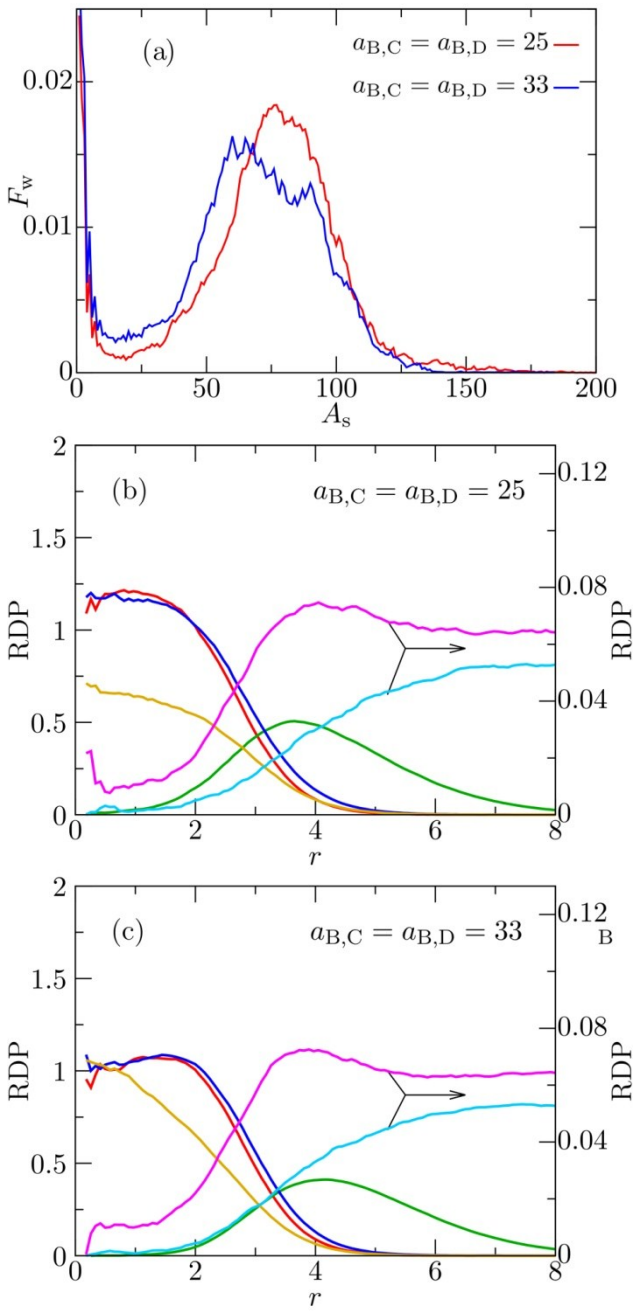

Figure S14. Systems containing 260 $A_5^+B_{15}$ chains, 347 C_5^- chains (charge ratio ξ=1.35) and 200 D_5. Part (a) Weight distribution function, $F_w(A_S)$, of co-assembled particles in mixtures with $a_{BC} = a_{BD} = 25$ (red curve) and $a_{BC} = a_{BD} = 33$ (blue curve). Parts (b) and (c) Radial density profiles for associates with A_S=60 for (b) $a_{BC} = a_{BD} = 25$ and (c) $a_{BC} = a_{BD} = 33$. The left-hand vertical axis and red curves correspond to A^+ beads, green ones to B beads, the blue ones stand for C^- beads and the ochre ones for D beads. The right-hand vertical axis corresponds to the counterion: magenta to positive ones and cyan to negative ones.

7.3. Simulations for systems with less soluble beads D.

The following part present supplementary data are for systems with interaction parameters: a_{BC} =a_{BD} = a_{AC} = a_{AD} = a_{BS} = a_{CD} = a_{BCI} = a_{SCI} = 25; a_{SA} =a_{SC} = a_{AB} = a_{CCI} = a_{ACI} = = 33 and a_{SD} = a_{DCI} = 40.

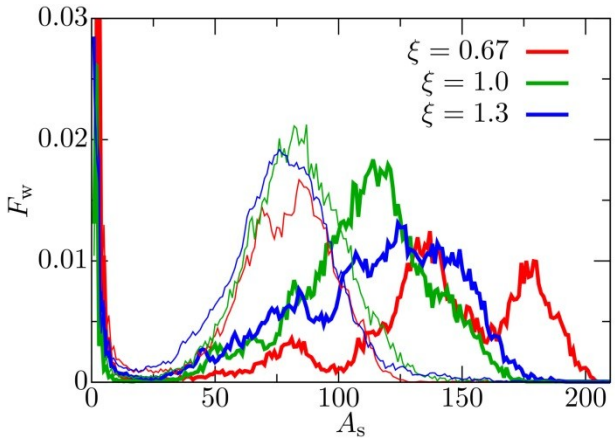

Figure S15. Weight distribution function, $F_w(A_S)$, of co-assembled particles in mixtures containing 200 D_5 chains and 260 $A_5^+B_{15}$ chains with several ratios of negative to positive charges, ξ, for interaction parameters a_{SD} =40 (thick curves) and a_{SD} =33 (thin curves).

7.4. Simulations for systems with less incompatible ions and counterions with core forming polymer beads

The following part present supplementary data for systems with interaction parameters: a_{AC} = a_{BC} = a_{BS} = a_{BCI} = a_{SCI} =*25;* a_{AB} =a_{AS} = a_{CS} = 33 and a_{ACI} = a_{CCI} = 27; 29; 31; 33.

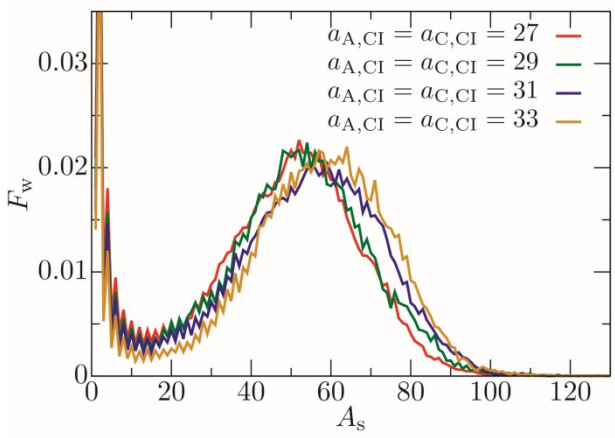

Figure S16. Weight distribution function, $F_w(A_S)$, of co-assembled particles in mixtures containing 260 $A_5^+B_{15}$ chains and 260 C_5^- chains (charge ratio ξ=1.00)

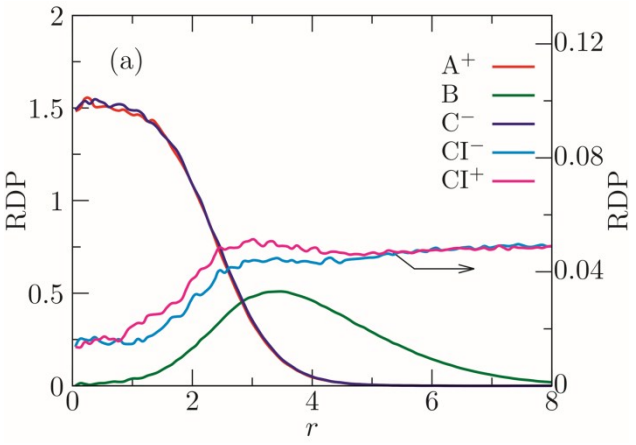
(a)
A+
B
C−
CI−
CI+
RDP
RDP
r

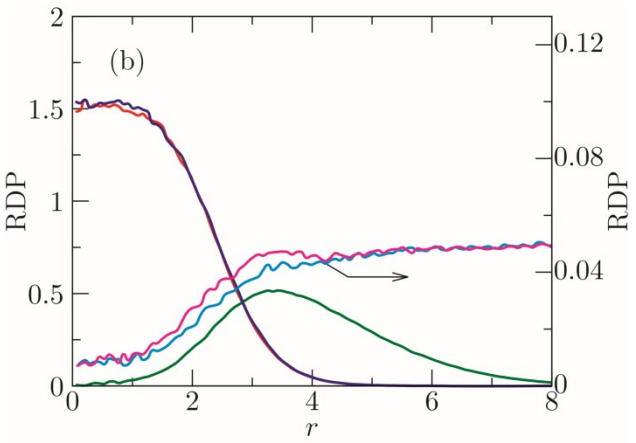
(b)
RDP
RDP
r

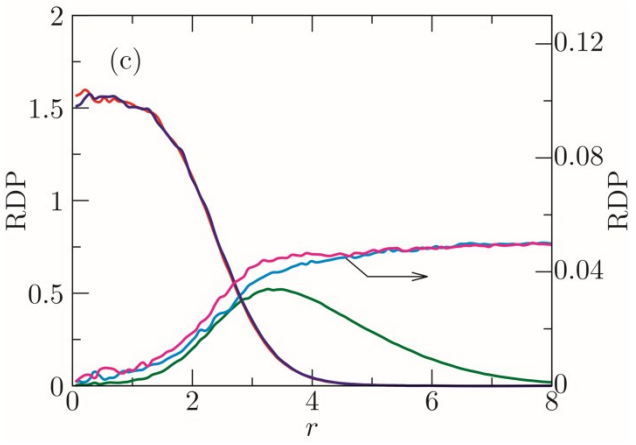
(c)
RDP
RDP
r

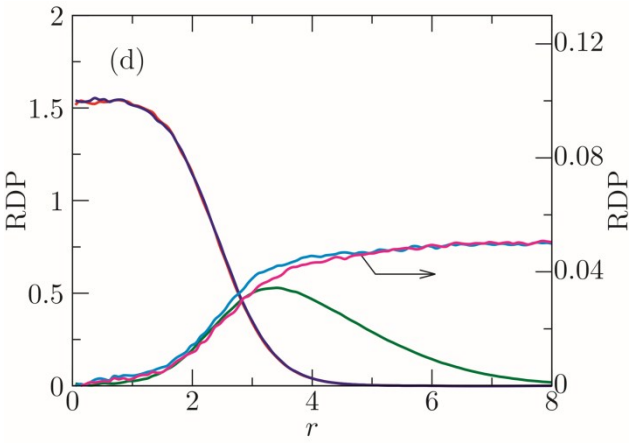

Figure S17. Radial density profiles for associates with A_s=50 in systems containing 260 $A_5^+B_{15}$ chains and 260 C_5^- chains for (a) $a_{ACI} = a_{CCI} = 27$, (b) $a_{ACI} = a_{CCI} = 29$, (c) $a_{ACI} = a_{CCI} = 31$ and (d) $a_{ACI} = a_{CCI} = 33$. The left-hand vertical axis and red curves correspond to A^+ beads, green ones to B beads and the blue ones stand for C^- beads. The right-hand vertical axis corresponds to the counterion: magenta to positive ones and cyan to negative ones.

Density profiles of counterions in the main paper (in Fig.3 and Fig.6) indicate that small ions escape in bulk solvent and that their concentration the IPC core is negligible. De Pablo[27] and Sing et.al[28] studied also the distribution of small ions and observed their finite concentration in IPC cores. The difference our results and the results of other authors is due to parameter setting. In most cases, we assume (for simplicity) that the counterions are fairly incompatible with the core-forming blocks. However, we are aware of the fact that the blocks in real systems contain a number of ionic (salt-forming) groups. Therefore we performed a parametric study by varying the repulsion between the core-forming beads A and C, and counterions CI from $a_{ACI} = a_{CCI} = 27$ (fairly compatible beads) to 31 (moderately incompatible beads). Results are briefly described and discussed in the main paper, but the appropriate RDP_i are shown and discussed here in ESI. (Figures S16 and S17). For the comfort, we reproduce a part of the text from the main paper. The comparison of density profiles shows that the relatively compatible ions ($a_{ACI} = a_{CCI} = 27$) penetrate in cores more than the incompatible ions, but their concentration in IPC cores is only three times higher than that of ions with $a_{ACI} = a_{CCI} = 31$, and this concentration (for $a_{ACI} = a_{CCI} = 27$) in cores is still two times lower than the concentration in the bulk solvent. The comparison of distributions of association numbers for different values $a_{ACI} = a_{CCI}$ shows that at low ionic strength (in systems without added salt), the compatibility/incompatibility of ions does not almost affect the association process. We addressed this problem also in our earlier studies[21] (see Fig. 15 in this paper). In summary, the results of both

studies have shown that at low ionic strength (in systems without added salt), the small ions try to escape into the bulk solvent as much as they can (because the increase in entropy is the main driving force of the electrostatic co-assembly) and the compatibility/incompatibility of small ions almost does not affect the co-assembly. In systems with added salt, the effects of compatible and incompatible ions differ (see Fig. 15 in the study[21]). In this case, the penetration of ions in IPC cores is promoted upon addition of the salt composed of compatible ions. These ions screen electrostatic repulsion and promote the dissociation of the co-assembled core-shell particles, i.e., the association number decreases. On the other hand, the addition of small incompatible ions does not almost affect the co-assembling process.

References

1. P. J. Hoogerbrugge and J. M. V. A. Koelman, *Europhysics Letters*, 1992, **19**, 155-160.
2. J. M. V. A. Koelman and P. J. Hoogerbrugge, *Europhysics Letters*, 1993, **21**, 363-368.
3. M. Rubinstein and R. H. Colby, *Polymer Physics*, New York: Oxford University, 2003.
4. P. Espanol and P. Warren, *Europhysics Letters*, 1995, **30**, 191-196.
5. R. D. Groot and P. B. Warren, *Journal of Chemical Physics*, 1997, **107**, 4423-4435.
6. M. Rubinstein and R. H. Colby, in *Polymer physics*, Oxford University, New York, 2003, ch. 4, pp. 137-170.
7. P. B. Warren and A. Vlasov, *Journal of Chemical Physics*, 2014, **140**.
8. C. Ibergay, P. Malfreyt and D. J. Tildesley, *Journal of Chemical Theory and Computation*, 2009, **5**, 3245-3259.
9. M. Gonzalez-Melchor, E. Mayoral, M. E. Velazquez and J. Alejandre, *Journal of Chemical Physics*, 2006, **125**.
10. R. D. Groot, *Journal of Chemical Physics*, 2003, **118**, 11265-11277.
11. M. Carrillo-Tripp, H. Saint-Martin and I. Ortega-Blake, *Journal of Chemical Physics*, 2003, **118**, 7062-7073.
12. M. A. Seaton, R. L. Anderson, S. Metz and W. Smith, *Molecular Simulation*, 2013, **39**, 796-821.
13. T. W. Kibble and F. H. Berkshire, *Classical Mechanics*, Imperial College Press, London, 5th edn., 2004.

14. J. Cesarano, I. A. Aksay and A. Bleier, *Journal of the American Ceramic Society*, 1988, **71**, 250-255.
15. Z. Posel, Z. Limpouchova, K. Sindelka, M. Lisal and K. Prochazka, *Macromolecules*, 2014, **47**, 2503-2514.
16. T. J. Martin, K. Prochazka, P. Munk and S. E. Webber, *Macromolecules*, 1996, **29**, 6071-6073.
17. K. Podhajecka, M. Stepanek, K. Prochazka and W. Brown, *Langmuir*, 2001, **17**, 4245-4250.
18. M. Stepanek, K. Podhajecka, K. Prochazka, Y. Teng and S. E. Webber, *Langmuir*, 1999, **15**, 4185-4193.
19. D. Kiserow, K. Prochazka, C. Ramireddy, Z. Tuzar, P. Munk and S. E. Webber, *Macromolecules*, 1992, **25**, 461-469.
20. M. Lisal, Z. Limpouchova and K. Prochazka, *Physical Chemistry Chemical Physics*, 2016, **18**, 16127-16136.
21. K. Sindelka, Z. Limpouchova, M. Lisal and K. Prochazka, *Macromolecules*, 2014, **47**, 6121-6134.
22. V. Dordovic, M. Uchman, K. Prochazka, A. Zhigunov, J. Plestil, A. Nykanen, J. Ruokolainen and P. Matejicek, *Macromolecules*, 2013, **46**, 6881-6890.
23. M. Stepanek, K. Podhajecka, E. Tesarova, K. Prochazka, Z. Tuzar and W. Brown, *Langmuir*, 2001, **17**, 4240-4244.
24. S. van der Burgh, A. de Keizer and M. A. C. Stuart, *Langmuir*, 2004, **20**, 1073-1084.
25. J. Rudnick and G. Gaspari, *Science*, 1987, **237**, 384-389.
26. M. Stepanek, K. Krijtova, K. Prochazka, Y. Teng, S. E. Webber and P. Munk, *Acta Polymerica*, 1998, **49**, 96-102.
27. L. Li, S. Srivastava, M. Andreev, A. B. Marciel, J. J. de Pablo and M. V. Tirrell, *Macromolecules*, 2018, **51**, 2988-2995.
28. S. L. Perry and C. E. Sing, *Macromolecules*, 2015, **48**, 5040-5053.